Journal of Hazardous Materials 192 (2011) 368–373

Contents lists available at ScienceDirect

Journal of Hazardous Materials

journal homepage: www.elsevier.com/locate/jhazmat

Gel-hydrothermal synthesis of carbon and boron co-doped TiO_2 and evaluating its photocatalytic activity

Yongmei Wu, Mingyang Xing, Jinlong Zhang*

Key Lab for Advanced Materials and Institute of Fine Chemicals, East China University of Science and Technology, 130 Meilong Road, Shanghai 200237, PR China

ARTICLE INFO

Article history:
Received 27 January 2011
Received in revised form 9 May 2011
Accepted 12 May 2011
Available online 19 May 2011

Keywords:
Co-doped
Photosensitization
Synergistic effect
Photocatalytic activity

ABSTRACT

Carbon and boron co-doped TiO_2 photocatalysts were prepared firstly by the gel-hydrothermal method, that is, synthesized through sol–gel process followed by hydrothermal in the glucose solution. The prepared photocatalysts were characterized by XRD, Raman spectra, TEM, N_2 physical adsorption, XPS, and UV–vis absorption spectra. It was found that the co-doped TiO_2 has a larger BET surface areas and a narrower band gap than undoped TiO_2. The experimental results show that the coke carbon generated on the carbon doped TiO_2 surface act as a photosensitizer and has the photosensitization effect under the visible light. Except for carbon sensitization effect, the boron and carbon co-doped TiO_2 has synergistic effect which is responsible for effective photo-degradation of 2,4-dichlorophenol in the visible light irradiation.

1. Introduction

As one of the semiconductor photocatalytic materials extensively used in the fields of environmental purification, titanium dioxide is most widely studied due to its advantages of inexpensiveness, chemical stability, and nontoxicity in addition to its favorable optoelectronic property [1,2]. However, its wide band gap (3.0–3.2 eV) allows it to absorb only the ultraviolet light which accounts for merely 5% of the solar photons, thereby hampering its wide applications. In order to utilize the solar energy efficiently, many studies on nonmetal element doping have been carried out to extend the spectral response of TiO_2 into the visible region and enhance its photocatalytic activity, such as N [3–6], C [7], S [8,9], P [10], halogen atoms [11–13] and B [14]. Among these anions doped TiO_2, boron doping TiO_2 attracted more attentions in the application studies of electrochemical and functional materials due to its prompting creation of electron acceptor level. Lambert et al. [15] have reported that low level of boron doping TiO_2 lead to significant absorption of visible light and better photoactivity for degradation of methyl tert-butyl ether (MTBE) than undoped TiO_2. Zaleska et al. [16] synthesized boron modified TiO_2 using boric acid and boric acid triethyl ester (BATE) by the sol–gel method and by grinding anatase powder with boron dopant. They found boron doping could result in absorption of the visible light and these B-TiO_2 samples have higher activity for photo-oxidation of phenol under the visible light irradiation than pure TiO_2. Except single boron doping, the co-doping of boron with other nonmetal element also has been studied in recent years. It was found that B and N co-doped TiO_2 [17], B and F co-doped TiO_2 [18] showed higher photocatalytic activity and peculiar characteristics compared with single element doping into TiO_2. However, few reports are published on B and C co-doped TiO_2 photocatalysts[19]. Our previous work have found that carbon modified TiO_2 presents high visible light performance and the carbon photosensitization plays an important role for its efficient visible light photocatalytic activity [20].

In this study, C and B co-doped TiO_2 photocatalysts were synthesized firstly by the gel-hydrothermal method, which showed efficient visible light photo-degradation of 2,4-dichlorophenol (2,4-DCP) compared with C-doped TiO_2 and B-doped TiO_2, resulting from the carbon and boron synergistic effect. Our significant work may provide new insights into the preparation of effective visible light photoactive TiO_2.

2. Experimental procedure

The carbon and boron co-doped TiO_2 was prepared by two steps process. Firstly, the boron doped TiO_2 was synthesized by sol–gel method. 6 ml tetrabutyl titanate was dissolved into 17 ml anhydrous ethanol (solution A), solution B consisted of 35 ml anhydrous ethanol, 0.1 ml concentrated nitric acid (68% weight percent), 1.6 ml water, 0.5 g PEG600 and 0.05 g H_3BO_3. Then solution A was added drop-wise to solution B under magnetic stirring. The resultant mixture was stirred at room temperature for 4 h until the transparent sol was obtained. The sol was then aged for 1 day and the gel

* Corresponding author. Tel.: +86 21 64252062; fax: +86 21 64252062.
E-mail address: jlzhang@ecust.edu.cn (J. Zhang).

0304-3894/$ – see front matter © 2011 Elsevier B.V. All rights reserved.
doi:10.1016/j.jhazmat.2011.05.037

was obtained. The gel was dried at 120 °C for 8 h to obtain B-doped amorphous TiO_2. Secondly, 0.75 g of amorphous B-doped TiO_2 and required amount of glucose (C/Ti = 0.16, 0.32, 0.48 mol%) were added into 50 ml of deionized water in a 100 ml Teflon-inner stainless steel autoclave. The autoclave was maintained at 180 °C for 10 h. The precipitate gained was washed by distilled water, dried at 100 °C for 24 h and calcined in the presence of air at 300 °C for 2 h in the muffle oven. The pure TiO_2 and B-doped TiO_2 were hydrothermal treated in the distilled water without glucose. The C-doped TiO_2 was also prepared in the presence of glucose solution (C/Ti = 0.16).

The structural properties were determined by X-ray diffractometer (a Rigaku D/max 2550 VB/PC) using graphite monochromatic copper radiation (Cu–Kα) at 40 kV and 100 mA over the 2θ range of 20–80°. BET surface area measurements were carried out by N_2 adsorption at 77 K using an ASAP2020 instrument. The binding energy was identified by X-ray photoelectron spectroscopy (XPS) with Mg Kα radiation (ESCALB MK-II). The UV–vis absorption spectra of samples were observed with Varian Cary 500 equipped with an integrating sphere. The surface morphologies and particle sizes were observed by high-resolution transmission electron microscopy (HRTEM, JEM-2011), using an accelerating voltage of 200 kV. Raman measurements were performed at room temperature using a Via + Reflex Raman spectrometer with the excitation wavelength of 514 nm.

2,4-Dichlorophenol (2,4-DCP) was selected as a target pollutant to evaluate the photocatalytic activity of prepared samples under visible light irradiation because there was no absorption for 2,4-DCP in the region of visible light. 0.05 g of photocatalyst was dispersed into a 50 ml 2,4-DCP aqueous solution (30 mg l^{-1}) and then irradiated with a 1000 W tungsten halogen lamp equipped with a UV cut-off filters (λ > 420 nm) under continuous stirring. The distance between the light and the reaction tube was fixed at 24 cm. The lamp was cooled with flowing water in a quartz cylindrical jacket around the lamp, and ambient temperature was maintained during the photocatalytic reaction because of good ventilation. Before the irradiation, the suspension was maintained in the dark for 1 h in order to reach the adsorption–desorption equilibrium. At each given time interval, about 4 ml suspensions was withdrawn, centrifuged and filtered to remove the remained particles. The concentration of 2,4-DCP was determined from the absorbance at the wavelength of 284 nm. For comparison, the same procedure was also done for commercial titania P25 (BET surface area 50 m^2/g^1).

3. Results and discussion

3.1. Characterization of carbon and boron co-doped TiO_2

Fig. 1 shows the XRD patterns of pure TiO_2, B-TiO_2, C-TiO_2, and (C, B)-TiO_2 with different carbon contents. The pure TiO_2 and B-TiO_2 contain trace amounts of brookite (JCPDS, No. 29-1360). However, C-TiO_2 and (C, B)-TiO_2 with different carbon contents consist of anatase as a unique phase (JCPDS, No. 21-1272), indicating that introducing carbon prohibits the formation of brookite. According to the line width analysis of the anatase (1 0 1) diffraction peak based on the Scherrer formula, the average crystalline sizes of all these samples are estimated and summarized in Table 1. All the samples have similar crystalline sizes of about 10 nm, which suggests that increasing carbon amount has little effect on the average crystalline sizes of co-doped TiO_2 due to the reason that most of carbon only possibly covered the surface or subsurface. It was reported that the presence of boron in the bulk of TiO_2 would result in lower crystallite dimensions [21]. When in the case of high B concentration, the boron ions could be expelled from the TiO_2 structure during the calcinations, forming a layer of diboron trioxide, which

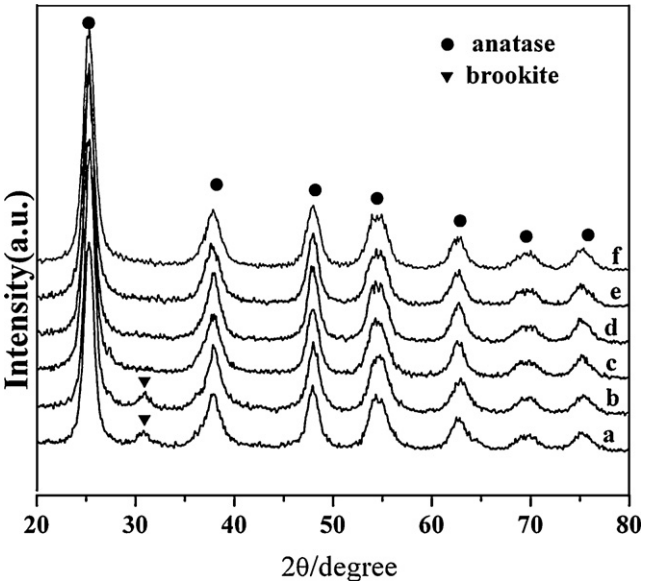

Fig. 1. XRD patterns of different samples: (a) TiO_2; (b) B-TiO_2; (c) C-TiO_2; (d) (0.16C, B)-TiO_2; (e) (0.32C, B)-TiO_2; and (f) (0.48C, B)-TiO_2.

retards the crystal growth [21]. However, in our study, no separate B_2O_3 phase was observed for any of the boron-containing samples, possibly due to the low B concentration. It is worth noting that at low B concentration, the effect of B on the crystal size and the crystal phase of TiO_2 are dependent on the preparation method (synthesis route, precursors, calcinations condition) [19,22]. Compared to undoped TiO_2, introducing B or co-doping with B and C have little effect on the average crystalline sizes of B doped TiO_2 and (C, B)-doped TiO_2, indicating that most of the B atoms only substitute for the surface or subsurface O atoms.

Raman spectra are divided into two parts: from 100 to 1000 cm^{-1} for the TiO_2 (Fig. 2(a)) and from 1000 cm^{-1} to 2000 cm^{-1} for the carbon structures (Fig. 2(b)). The Raman spectra of (0.32C, B)-TiO_2 are characterized by a strong band at 144 cm^{-1}, three bands at 394 cm^{-1}, 514 cm^{-1} and 638 cm^{-1}, which can be assigned to the fundamental vibration modes of anatase TiO_2 with the symmetries of E_g, B_{1g}, A_{1g} and E_g [23], respectively. The bands at 1400 cm $^{-1}$ and 1600 cm $^{-1}$ in Fig. 2(b) are from coke species [24]. Some other researchers also found that surface-bound coke was easier to generate when using glucose as the carbon source through gel-calcination method [25].

Fig. 3(a) shows the TEM images of the (0.32C, B)-doped TiO_2 sample calcined at 300 °C. The image shows that sample consists of large number of small particles with the size of around 10 nm, which is in the agreement with the XRD results calculated by the Scherrer equation. Fig. 3(b) shows the nitrogen adsorption–desorption isotherms and pore size distribution curves (inset) of the (0.32C, B)-TiO_2 sample. The adsorption isotherm can be classified as type IV with hysteresis loops in the IUPAC classification, which is characteristic of mesoporous materials [26]. The pore size distribution is calculated from desorption branch of a nitrogen isotherm by the Barret–Joyner–Halenda (BJH) method using the Halsey equation. The pore size distribution of (0.32C, B)-TiO_2 sample is shown in the inset of Fig. 3. It reveals that the average pore size is about 3.1 nm. The other samples have the similar N_2 adsorption–desorption isotherms and BJH pore size distributions to (0.32C, B)-TiO_2 sample (not shown). Their textural properties are listed in Table 1. Compared to pure TiO_2 (115 m^2/g) and B-TiO_2 (108 m^2/g), the surface areas of C-TiO_2 and (C, B)-TiO_2 increased significantly due to their hydrothermal treatment in different solutions. The undoped TiO_2 and B-TiO_2 samples were treated in the

Table 1
Crystallite size, band gap and textural properties of different samples.

Sample	Crystallite size (nm)	Specific surface area (m^2/g)	Pore diameter (nm)	Pore volume (cm^3/g)	E_g (eV)
TiO_2	9.9	115	4.2	0.215	3.10
B-TiO_2	10.1	108	4.2	0.206	2.95
C-TiO_2	9.9	171	2.7	0.219	2.55
(0.16C, B)-TiO_2	10.3	164	3.1	0.212	2.47
(0.32C, B)-TiO_2	10.1	205	3.5	0.234	2.39
(0.48C, B)-TiO_2	9,8	113	3.2	0.134	1.97

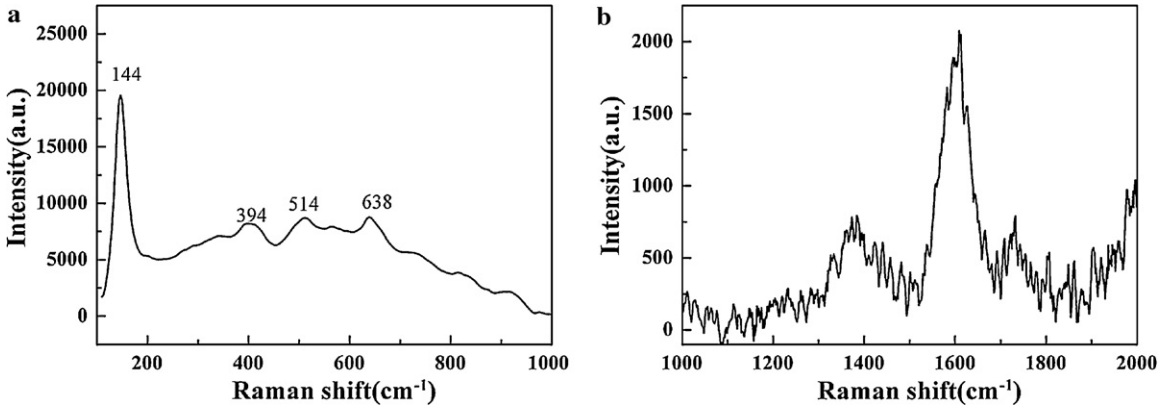

Fig. 2. Raman spectra (a) and (b) for (0.32C, B)-TiO_2.

distilled water, while both C-TiO_2 and (C, B)-TiO_2 samples were hydrothermalled in the presence of glucose solution. The (0.32C, B)-TiO_2 sample has the highest BET surface areas of 204 m^2/g. However, the BET surface area of the (0.48C, B)-TiO_2 sample decreases intensively to about 113 m^2/g, and its pore volume also drops to 0.134 cm^3/g, indicating that increased carbon amount might result in the aggregation of the particles.

Fig. 4(a) shows the XPS spectrum for B 1s of (0.32C, B)-TiO_2. We know that the XPS is a surface inspection measurement. All the structures detected by the XPS are present on the catalyst surface or subsurface. The B 1s appears at the binding energy of 189.2 eV and 191.2 eV, which are ascribed to a substitutional B occupying O sites (O–Ti–B) and interstitial boron atoms (Ti–O–B) in the bulk of anatase, respectively [15,27,28]. As it is known that the complete substitutional B of B–Ti–B bond shows the characteristic peak at 197.5 eV, and the boron oxides of B_2O_3 presents the peak at 193.0 eV [28]. However, in our investigation the peak shifts from 187.5 to 189.2 eV due to the higher electronegativity of O than B, resulting to the incomplete substitutional B occupying only one O site to form the O–Ti–B bond. Identically, the Ti–O–B formation also induces the peak change from 193.0 to 191.2 eV due to the high electron supplying capacity of Ti atom. Moreover, the above results are consistent with the DFT calculation results proposed by Di Valentin et al. [29]. They found both substitutional and interstitial B atoms are all stable existence in the bulk of anatase after annealing at high temperature on the basis of DFT calculation. Fig. 4(b) shows the XPS spectrum for C 1s of (0.32C, B)-TiO_2. After using Gaussian peak fitting, the deconvoluted XPS spectra present three peaks at 284.6, 285.3 and 288.2 eV. The lower binding energy at 284.6 eV is associated with the adventitious elemental carbon [30]. The second peak at 285.3 eV can be assigned to coke carbon [31], which is confirmed by the Raman spectra results. The small peak at 288.2 eV suggest the existence of C=O and COO [20]. Therefore, there are two different carbon species existing in the co-doping samples, one is surface coke carbon and another is carbonate species. The former is with major responsibility for its visible light response.

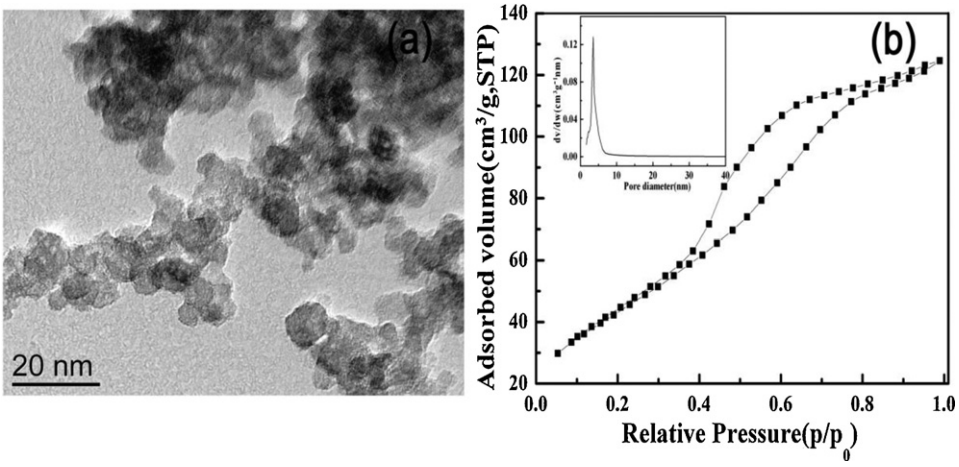

Fig. 3. TEM image (a) for (0.32C, B)-TiO_2 and N_2 adsorption–desorption isotherm (b) and BJH pore size distribution curve (inset) of (0.32C, B)-TiO_2.

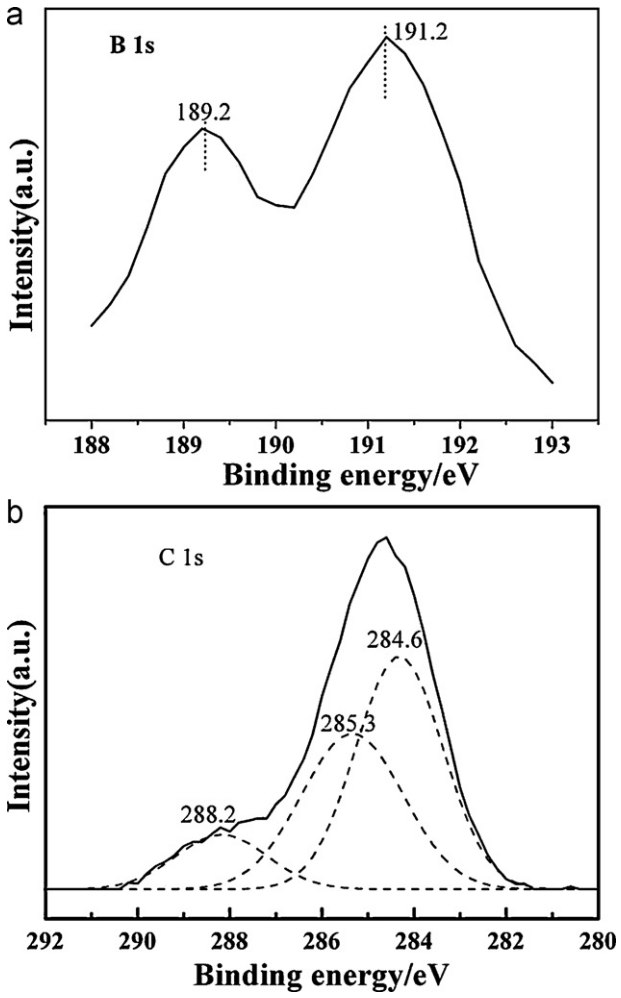

Fig. 4. XPS spectra of (0.32C, B)-TiO_2: (a) B 1s and (b) C 1s.

The optical properties of different samples were investigated by the UV–vis absorption spectroscopy as shown in Fig. 5. The band gaps of samples were also estimated from the intercept of UV–vis spectra by the equation ($E_g = 1240/\lambda$) (see Table 1). Pure TiO_2 has the band energy of 3.10 eV, while B-doped TiO_2 shows a little red shift to 2.95 eV. The origin of absorption bands in the visible spectral range for anion doped TiO_2 specimens remains a hot topic of discussion. It was reported that anion modification in titania increased visible light absorption by the introduction of localized states in the band gap [32]. While some of studies revealed that intrinsic defects, including those defects associated with oxygen vacancies, contributed to the absorption of light in the visible spectral region [33]. A recent study by Kuznetsov and Serpone has proposed that the commonality in all these doped titania rested with formation of oxygen vacancies and the advent of color centers that absorb the visible light radiation [34]. Gopal et al. have proposed that B atom in the interstitial position TiO_2 favors formation of oxygen with two excess electrons, which would further reduced from Ti^{4+} ions to Ti^{3+} [35]. Therefore we assume that B doping may lead to increase the formation of oxygen vacancies, which is responsible for the red shifted optical absorption. However, a noticeable shift of absorption edge to the visible light region was observed for C-TiO_2, and (C, B)-TiO_2 samples compared with pure TiO_2 and B-TiO_2. Moreover, the absorption of co-doped sample increases with increasing of carbon content in the visible light region, which indicates the carbon dopant is responsible for its strong visible light response. Our XPS results also demonstrate the presence of substitutional B atoms and coke carbon, which result in the visible light absorption and band gap reduction for co-doped samples due to the synergistic effect between substitutional boron and coke carbon discussed as follows.

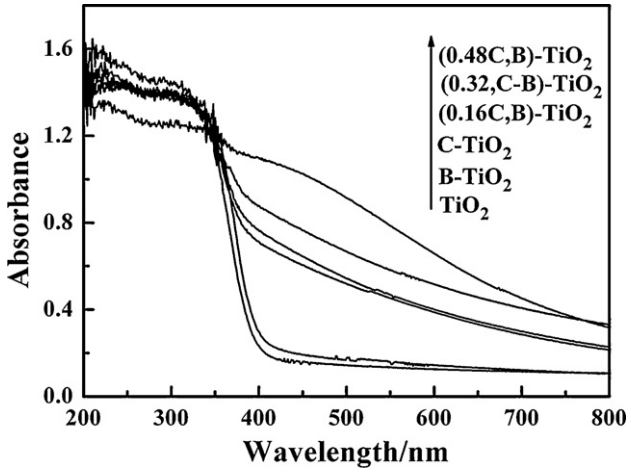

Fig. 5. UV–vis absorption spectra of all samples.

3.2. Photocatalytic activity

The visible photocatalytic activity of C and B co-doped TiO_2 samples were evaluated by measuring the decomposition of 2,4-DCP under visible light irradiation ($\lambda > 420$ nm) for 5 h. P25 as a typical reference TiO_2 was used for comparison. Fig. 6(a) shows the concentration change of 2,4-DCP for different samples against the reaction time. The photocatalytic degradation of 2,4-DCP with reaction time is first order as confirmed by the linear transforms of $\ln(C_0/C) \sim t$ shown in Fig. 6(b), from which the apparent rate constants can be obtained. The apparent rate constants obtained with various catalyst samples are shown in Table 2. It can be seen that the degradation rate of pure TiO_2 and P25 is very low due to their bigger band-gap energy [36]. After B introduction into TiO_2, its photocatalytic activity has a little increase. That is because of only a little narrowed band gap caused by the substitutional B doping (see Table 1). However, after carbon doping, samples exhibit much higher degradation rates for 2,4-DCP compared with pure TiO_2, P25 and B-TiO_2. During the photo-degradation process of carbon doped samples, surface coke carbon acted as a photosensitizer, which can absorb visible light and generate photo-excited electrons. These excited electrons are injected into the TiO_2 conduction band (CB) to form Ti^{3+}, $O_2^{\bullet -}$, $^{\bullet}OH$ and other reactive superoxide species, resulting in the oxidation of 2,4-DCP as shown in Scheme 1 [37]. Therefore, coke species coating on the surface of TiO_2 are likely to carry out a charge transfer process and responsible for its photosensitized photocatalysis. It is noteworthy that the degradation rate of 2,4-DCP is further enhanced by the carbon co-doped with boron, and the (0.32C, B)-TiO_2 presents high photocatalytic activity. To B and C co-doped TiO_2, the boron and carbon synergistic effect plays an important role in the photocatalytic process. From B 1s XPS results, the presence of substitutional B atoms indicates the oxygen atom in TiO_2 is substituted by boron and a narrow substitute band is formed above valence band (VB). Simultaneously, the sensitization effect of surface coke carbon induces Ti^{3+} level generated below the CB [35,38]. As a result, the band energy of TiO_2 is lowered by a significant shift, which induces the easier transition of photo-excited electrons from boron dopant level to the Ti^{3+} level as shown in Scheme 1. Thereby, the carbon sensitization effect com-

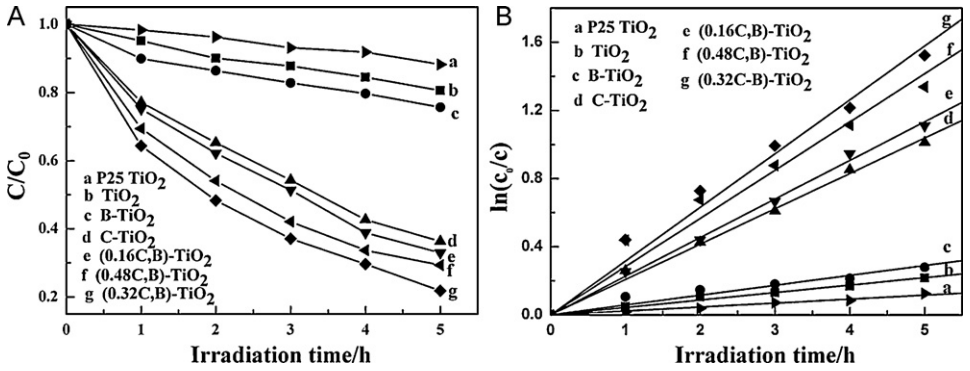

Fig. 6. Photodegradation of 2,4-DCP using different samples under visible light irradiation for 5 h: (a) $C/C_0 \sim t$ and (b) $\ln(C_0/C) \sim t$.

Table 2
The apparent rate constant (k_a) of all samples and their comparison with that of P25.

Sample	P25	TiO_2	B-TiO_2	C-TiO_2	(0.16C, B)-TiO_2	(0.32C, B)-TiO_2	(0.48C, B)-TiO_2
k_a ($\times 10^{-2}$, h^{-1})	2.32	4.37	5.79	20.75	22.67	31.55	28.30

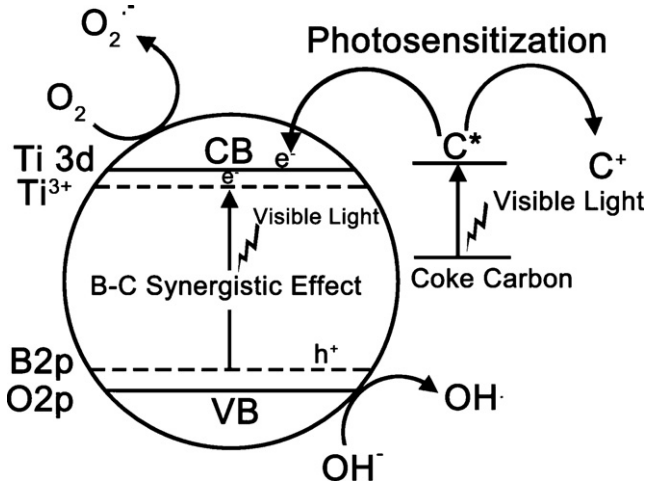

Scheme 1. Mechanism for the synergistic effect of carbon and boron.

bination with boron and carbon synergistic effect are responsible for its efficient photocatalytic activity of (C, B)-TiO_2.

4. Conclusions

Carbon and boron co-doped TiO_2 photocatalysts with larger surface area were prepared by the gel-hydrothermal method for the first time. The co-doped TiO_2 samples exhibit a stronger adsorption in visible-light region than pure TiO_2. To the carbon doped TiO_2, surface coke carbon photosensitization effect is responsible for its high photocatalytic activity in the visible light irradiation. When carbon is co-doped with boron, the carbon photosensitization and B–C synergistic effects play a major role in its efficient photo-degradation of 2,4-DCP under the visible light. Furthermore, the (0.32C, B)-TiO_2 showed highest photocatalytic activity, which was eight times higher than that of undoped TiO_2.

Acknowledgments

This work has been supported by National Nature Science Foundation of China (20773039, 20977030), National Basic Research Program of China (973 Program, 2007CB613301, 2010CB732306), Science and Technology Commission of Shanghai Municipality (10520709900, 10JC1403900) and the Fundamental Research Funds for the Central Universities.

References

[1] M.R. Hoffmann, S.T. Martin, W. Choi, D.W. Bahnemann, Environmental applications of semiconductor photocatalysis, Chem. Rev. 95 (1995) 69–96.
[2] I. Catanzaro, G. Avellone, G. Marc, M. Saverini, L. Scalici, G. Sciandrello, L. Palmisano, Biological effects and photodegradation by TiO_2 of terpenes present in industrial wastewater, J. Hazard. Mater. 185 (2011) 591–597.
[3] R. Asahi, T. Morikawa, T. Ohwaki, K. Aoki, Y. Taga, Visible-light photocatalysis in nitrogen-doped titanium oxides, Science 293 (2001) 269–271.
[4] Y. Cong, J. Zhang, F. Chen, M. Anpo, Synthesis and characterization of nitrogen-doped TiO_2 nanophotocatalyst with high visible light activity, J. Phys. Chem. C 111 (2007) 6976–6982.
[5] M. Xing, J. Zhang, F. Chen, New approaches to prepare nitrogen-doped TiO_2 photocatalysts and study on their photocatalytic activities in visible light, Appl. Catal. B: Environ. 89 (2009) 563–569.
[6] Y.F. Ma, J.L. Zhang, B.Z. Tian, F. Chen, L.Z. Wang, Synthesis and characterization of thermally stable Sm, N co-doped TiO_2 with highly visible light activity, J. Hazard. Mater. 182 (2010) 386–393.
[7] S. Sakthivel, H. Kisch, Daylight photocatalysis by carbon-modified titanium dioxide, Angew. Chem. Int. Ed. 42 (2003) 4908–4911.
[8] H.M. Luo, T. Takata, Y.G. Lee, J.F. Zhao, K. Domen, Y.S. Yan, Photocatalytic activity enhancing for titanium dioxide by co-doping with bromine and chlorine, Chem. Mater. 16 (2004) 846–849.
[9] Y. Wang, Y. Huang, W. Ho, L. Zhang, Z. Zou, S. Lee, Biomolecule-controlled hydrothermal synthesis of C–N–S-tridoped TiO_2 nanocrystalline photocatalysts for NO removal under simulated solar light irradiation, J. Hazard. Mater. 169 (2009) 77–87.
[10] L. Lin, W. Lin, J.L. Xie, Y.X. Zhu, B.Y. Zhao, Y.C. Xie, Photocatalytic properties of phosphor-doped titania nanoparticles, Appl. Catal. B: Environ. 75 (2007) 52–58.
[11] D. Li, H. Haneda, S. Hishita, N. Ohashi, Visible-light-driven N–F-codoped TiO_2 photocatalysts. 1. Synthesis by spray pyrolysis and surface characterization, Chem. Mater. 17 (2005) 2588–2595.
[12] D. Li, H. Haneda, S. Hishita, N. Ohashi, Visible-light-driven N–F-codoped TiO_2 photocatalysts. 2. Optical characterization, photocatalysis, and potential application to air purification, Chem. Mater. 17 (2005) 2596–2602.
[13] S. Chen, Y. Yang, W. Liu, Preparation, characterization and activity evaluation of TiN/F–TiO_2 photocatalyst, J. Hazard. Mater. 186 (2011) 1560–1567.
[14] M. Xing, Y. Wu, J. Zhang, F. Chen, Effect of synergy on the visible light activity of B, N and Fe co-doped TiO_2 for the degradation of MO, Nanoscale 2 (2010) 1233–1239.
[15] S. In, A. Orlov, R. Berg, F. Garcia, S. Pedrosa-Jimenez, M.S. Tikhov, D.S. Wright, R.M. Lambert, Effective visible light-activated B-doped and B, N-codoped TiO_2 photocatalysts, J. Am. Chem. Soc. 129 (2007) 13790–13791.
[16] A. Zaleska, E. Grabowska, J.W. Sobczak, M. Gazda, J. Hupka, Photocatalytic activity of boron-modified TiO_2 under visible light: the effect of boron content, calcination temperature and TiO_2 matrix, Appl. Catal. B: Environ. 89 (2009) 469–475.
[17] G. Liu, Y. Zhao, C. Sun, F. Li, G.Q. Lu, H.-M. Cheng, Synergistic effects of B/N doping on the visible-light photocatalytic activity of mesoporous TiO_2, Angew. Chem. Int. Ed. 47 (2008) 4516–4520.
[18] E.A. Reyes-Garcia, Y.P. Sun, D. Raftery, Solid-state characterization of the nuclear and electronic environments in a boron–fluoride co-doped TiO_2 visible-light photocatalyst, J. Phys. Chem. C 111 (2007) 17146–17154.

[19] Y. Wu, M. Xing, J. Zhang, F. Chen, Effective visible light-active boron and carbon modified TiO_2 photocatalyst for degradation of organic pollutant, Appl. Catal. B: Environ. 97 (2010) 182–189.
[20] J. Zhong, F. Chen, J.L. Zhang, Carbon-deposited TiO_2: synthesis, characterization, and visible photocatalytic performance, J. Phys. Chem. C 114 (2010) 933–939.
[21] D. Chen, D. Yang, Q. Wang, Z. Jiang, Effects of boron doping on photocatalytic activity and microstructure of titanium dioxide nanoparticles, Ind. Eng. Chem. Res. 45 (2006) 4110–4116.
[22] V. Gombac, L.D. Rogatis, A. Gasparotto, G. Vicario, T. Montini, D. Barreca, G. Balducci, P. Fornasiero, E. Tondello, M. Graziani, TiO_2 nanopowders doped with boron and nitrogen for photocatalytic applications, Chem. Phys. 339 (2007) 111–123.
[23] H. Berger, H. Tang, F. Lévy, Growth and Raman spectroscopic characterization of TiO_2 anatase single crystals, J. Cryst. Growth 130 (1993) 108–112.
[24] C. Li, P.C. Stair, Ultraviolet Raman spectroscopy characterization of coke formation in zeolites, Catal. Today 33 (1997) 353–360.
[25] C. Lettmann, K. Hildenbrand, H. Kisch, W. Macyk, W.F. Maier, Visible light photodegradation of 4-chlorophenol with a coke-containing titanium dioxide photocatalyst, Appl. Catal. B: Environ. 32 (2001) 215–227.
[26] K.S.W. Sing, D.H. Everett, R.A.W. Haul, L. Moscou, R.A. Pierotti, J. Rouquerol, T. Sieminewska, Reporting physisorption data for gas/solid systems with special reference to the determination of surface area and porosity, Pure Appl. Chem. 57 (1985) 603–619.
[27] Y. Huo, X. Zhang, Y. Jin, J. Zhu, H. Li, Highly active $La_2O_3/Ti_{1-x}B_xO_2$ visible light photocatalysts prepared under supercritical conditions, Appl. Catal. B: Environ. 83 (2008) 78–84.
[28] W. Zhao, W. Ma, C. Chen, J. Zhao, Z. Shuai, Efficient degradation of toxic organic pollutants with $Ni_2O_3/TiO_{2-x}B_x$ under visible irradiation, J. Am. Chem. Soc. 126 (2004) 4782–4783.
[29] E. Finazzi, C. Di Valentin, G. Pacchioni, Boron-doped anatase TiO_2: pure and hybrid DFT calculations, J. Phys. Chem. C 113 (2009) 220–228.
[30] S.Y. Treschev, P.-W. Chou, Y.-H. Tseng, J.-B. Wang, E.V. Perevedentseva, C.-L. Cheng, Photoactivities of the visible-light-activated mixed-phase carbon-containing titanium dioxide: the effect of carbon incorporation, Appl. Catal. B: Environ. 79 (2008) 8–16.
[31] K. Nagaveni, M.S. Hegde, N. Ravishankar, G.N. Subbanna, G. Madras, Synthesis and structure of nanocrystalline TiO_2 with lower band gap showing high photocatalytic activity, Langmuir 20 (2004) 2900–2907.
[32] X. Chen, C. Burda, The electronic origin of the visible-light absorption properties of C-, N- and S-doped TiO_2 nanomaterials, J. Am. Chem. Soc. 130 (2008) 5018–5019.
[33] N. Serpone, Is the band gap of pristine TiO_2 narrowed by anion- and cation-doping of titanium dioxide in second-generation photocatalysts? J. Phys. Chem. B 110 (2006) 24287–24293.
[34] V.N. Kuznetsov, N. Serpone, On the origin of the spectral bands in the visible absorption spectra of visible-light-active TiO_2 specimens analysis and assignments, J. Phys. Chem. C 113 (2009) 15110–15123.
[35] N.O. Gopal, H.H. Lo, S.C. Ke, Chemical state and environment of boron dopant in B,N-codoped anatase TiO_2 nanoparticles: an avenue for probing diamagnetic dopants in TiO_2 by electron paramagnetic resonance spectroscopy, J. Am. Chem. Soc. 130 (2008) 2760–2761.
[36] A.G. Agrios, K.A. Gray, E. Weitz, Photocatalytic transformation of 2,4,5-trichlorophenol on TiO_2 under sub-band-gap illumination, Langmuir 19 (2003) 1402–1409.
[37] Z. Lin, A. Orlov, R.M. Lambert, M.C. Payne, New insights into the origin of visible light photocatalytic activity of nitrogen-doped and oxygen-deficient anatase TiO_2, J. Phys. Chem. B 109 (2005) 20948–20952.
[38] C. Di Valentin, G. Pacchioni, A. Selloni, Theory of carbon doping of titanium dioxide, Chem. Mater. 17 (2005) 6656–6665.